Journal of Magnetics 17(3), 190-195 (2012) http://dx.doi.org/10.4283/JMAG.2012.17.3.190

Comparative Analysis on Magnetic Field and Inductances of Slotless Permanent Magnet Machine with Two Types of Winding based on Analytical Method

Seok-Myeong Jang*, Jeong-Man Kim, Jae-Hoon Jeong, Cheol Han, Ji-Hun Ahn, Duk-Jin Chang, and Hyun-Jun Park

Department of Electrical Engineering, Chungnam National University, Daejeon 305-764, Korea

(Received 24 April 2012, Received in final form 30 July 2012, Accepted 31 July 2012)

This paper presents an analytical approach to the magnetic field and the inductances of slotless permanent magnet machines with two types of winding. On the basis of a magnetic vector potential and a two-dimensional polar system, analytical solutions for flux density due to a permanent magnet and current are obtained. In addition, self and mutual inductances are obtained using the energy relationship. The analytical results are extensively validated by the nonlinear finite element method and by experimental results.

Keywords : inductance, slotless, winding type

1. Introduction

Due to their high power density, high efficiency, and low maintenance costs, permanent magnet machines are emerging as a key technology for various applications such as home appliances, industrial tools, and electric vehicles [1, 2].

The self and mutual inductances can have an important influence on both the steady-state and transient dynamic performance of a machine. As in any electric circuit, the inductance plays an important role in determining a motor's characteristics [2-4].

In high-speed conditions, the inductance may limit the rate of the rise in current, with the result that the desired current is never reached. In order to, high inductances can cause a deteriorated torque-speed curve that is significantly different from the ideal linear characteristic, which may necessitate advancing the commutation in order to increase the high-speed torque. Low inductances, on the other hand, can result in an excessive ripple current in pulse width modulation (PWM) controlled drive systems, which increases the motor losses and torque ripple [5-7].

Methods for the electromagnetic analysis of electric machines are widely classified in two categories: numerical methods and analytical methods, such as the space harmonic method. Numerical methods such as the finite element (FE) method provide an accurate means of determining the field distribution, taking due account of saturation, etc., but they remain time-consuming. The latter provide as much insight as analytical solutions into the influence of the design parameters on a machine's behavior [8-11].

The common types of winding in electrical machines are classified into two types: concentrated winding and distributed winding. Therefore, this paper deals with an analytical approach to the magnetic field, back-EMF, and inductances of a slotless permanent magnet machine with two types of winding, based on electromagnetic field theory. In addition, all the analytical results are validated using a two-dimensional (2-D) FE method that employs the commercial package ANSOFT MAXWELL.

2. Armature Reaction Analysis of Slotless Permanent Magnet (PM) motor

2.1. Analytical Model

Fig. 1(a) shows the analysis model with a four-pole, three-phase slotless permanent magnet synchronous motor with distributed winding. Its current modeling for an analytical approach is presented in Fig. 1(b).

Fig. 2(a), on the other hand, shows the analysis model with identical design specifications, but with concentrated winding. Its current modeling for an analytical approach is shown in Fig. 2(b).

*Corresponding author: Tel: +82-42-821-7608
Fax: +82-42-822-4933, e-mail: smjang@cnu.ac.kr

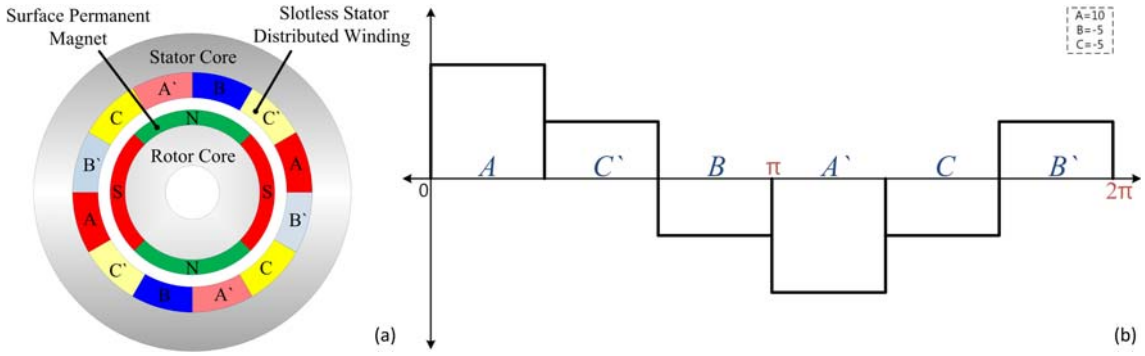

Fig. 1. (Color online) Slotless stator PM motor with distributed winding: (a) analytical model, and (b) current modeling.

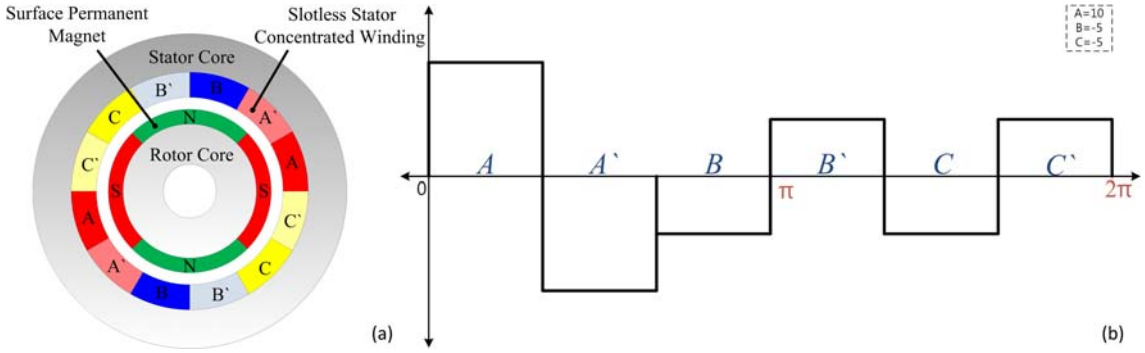

Fig. 2. (Color online) Slotless stator PM motor with concentrated winding: (a) analytical model, and (b) current modeling.

2.2. Current Density Modeling According to Winding Type

Fig. 1(b) and Fig. 2(b) show the Fourier series models for armature current modeling for distributed and concentrated windings.

$$\mathbf{J}_a(\theta) = \sum_{n=-\infty,odd}^{\infty} iI_n e^{-jnp_s\theta}\mathbf{i}_z \tag{1}$$

$$\mathbf{J}_b(\theta) = \sum_{n=-\infty,odd}^{\infty} -\frac{i}{2}I_n e^{-jnp_s\left(\theta-\frac{2\pi}{3}\right)}\mathbf{i}_z \tag{2}$$

$$\mathbf{J}_b(\theta) = \sum_{n=-\infty,odd}^{\infty} -\frac{i}{2}I_n e^{-jnp_s\left(\theta-\frac{2\pi}{3}\right)}\mathbf{i}_z \tag{3}$$

Here $\mathbf{J}_a$, $\mathbf{J}_b$, and $\mathbf{J}_c$ are the Fourier coefficients for each phase, and n and p_s are the harmonic order and the number of pole pairs, respectively. The distributed winding and concentrated winding coefficients can be obtained by (4).

$$\begin{aligned} I_{n(\text{Distributed})} &= -\frac{N_t}{jnp_sS}\left(e^{-jn\frac{1}{6}\pi} - 1 - e^{-jn\frac{2}{3}\pi} + e^{-jn\frac{1}{2}\pi}\right) \\ I_{n(\text{Concentrated})} &= -\frac{N_t}{jnp_sS}\left(e^{-jn\frac{1}{6}\pi} - 1 - e^{-jn\frac{2}{6}\pi} + e^{-jn\frac{1}{3}\pi}\right) \end{aligned} \tag{4}$$

Here, N_t is the number of turns per coil, and S is the area of the slot. Therefore, the current density **J** for stator winding can be expressed as (5):

$$\mathbf{J} = \mathbf{J}_a+\mathbf{J}_b+\mathbf{J}_c = \sum_{n=-\infty,odd}^{\infty} iI_n\left(e^{-jnp_s\theta} - \frac{1}{2}e^{-jnp_s\left(\theta-\frac{2\pi}{3}\right)} - \frac{1}{2}e^{-jnp_s\left(\theta-\frac{4\pi}{3}\right)}\right)\mathbf{i}_z \tag{5}$$

2.3. Magnetic Field Analysis by Armature Reaction Field

As shown in Fig. 3, for the convenience of the analytic approach, this paper suggests a 2-D analysis model that expresses each region with its own material property. Based on this 2-D analysis model and *Maxwell's equations*, the magnetic field analysis was performed. The magnetic vector potential for the analysis model in Cartesian coordinates is expressed by (6) [1].

$$\mathbf{A} = \text{Re}\, A_{zn}(r,t)e^{j(np_s\theta+mz)}\mathbf{i}_z \tag{6}$$

For the magnetic field analysis for PM, the coil is considered as air, and the flux density for the back-EMF derivation is obtained in the air-gap region. For the armature reaction field analysis for the winding current, on the other hand, the PM is considered as air, and the magnetic vector potential for the inductance derivation is

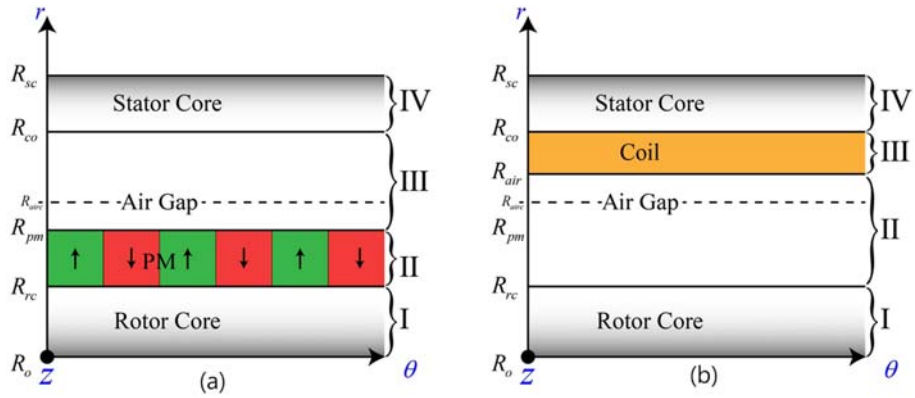

Fig. 3. (Color online) Simplified conceptual model for 2-D analytical method for (a) PM and (b) current.

obtained on the PM surface. In [9], analytical field solutions for a permanent magnet machine were presented that employ magnet pole shape modeling for the accuracy of the analysis, and the reliability of this modeling was proved. Hence, this paper refers to magnet pole shape modeling for the accuracy of its analysis.

In this analysis model, PM magnetization is defined as (7-1), and the mathematical modeling of the armature current is expressed by (7-2). Here, M_{rn} is the Fourier coefficient of magnetization in the radial direction, and J_{zn} is the current density.

$$\mathbf{M}_n = \sum_{n=-\infty,odd}^{\infty} \{M_{rn}e^{-jnp_s\theta}\mathbf{i}_r + M_{\theta n}e^{-jnp_s\theta}\mathbf{i}_\theta\} \tag{7-1}$$

$$\mathbf{J} = \sum_{n=-\infty,odd}^{\infty} J_{zn}e^{jnp_s\theta}\mathbf{i}_z \tag{7-2}$$

In the PM region, where the current does not exist, and in the coil region, where it does exist, the Poisson equation can be obtained as (8-1) and (8-2), based on Maxwell's equations. Here, $B = \nabla \times A$, based on the definition of the magnetic vector potential.

$$\nabla \times \mathbf{H}=0,\ \nabla^2\mathbf{A}_n=\mu\left\{\frac{jnp_s}{r}\left(M_n-\frac{M_{\theta n}}{jnp_s}\right)e^{jnp_s\theta}\right\} \tag{8-1}$$

$$\nabla \times \mathbf{H}=\mathbf{J},\ \nabla^2\mathbf{A}_n=-\mu_0\mathbf{J} \tag{8-2}$$

By calculating the above equations, the governing equation can be obtained. The governing equation in the PM magnetic field can be derived as (9-1), and that in the armature reaction field can be obtained as (9-2). Here, r is the radial length.

$$\left(\frac{\partial^2}{\partial r^2}A_{zn}+\frac{1}{r}\frac{\partial}{\partial r}A_{zn}-\left(\frac{np_s}{r}\right)^2A_{zn}\right)e^{jnp_s\theta}=\mu_0\left\{\frac{e^{jnp_s}}{r}M_ne^{jnp_s\theta}\right\} \tag{9-1}$$

$$\left(\frac{\partial^2}{\partial r^2}A_{zn}+\frac{1}{r}\frac{\partial}{\partial r}A_{zn}-\left(\frac{np_s}{r}\right)^2A_{zn}\right)e^{jnp_s\theta}=-\mu_0J_{zn}e^{jnp_s\theta} \tag{9-2}$$

The general solution can be achieved by solving the homogeneous solution and particular solution in that governing equation. (10-1) and (10-2) present the general solution in the PM magnetic field and the armature reaction field, respectively.

$$A_{znPM} = \sum_{n=-\infty,odd}^{\infty} (A_0r^{np_s} + B_0^{-np_s} + A_{znpPM})e^{jnp_s\theta} \tag{10-1}$$

$$A_{znAR} = \sum_{n=-\infty,odd}^{\infty} (C_0r^{np_s} + D_0^{-np_s} + A_{znpAR})e^{jnp_s\theta} \tag{10-2}$$

Here A_0, B_0, C_0, and D_0 are the coefficients determined by the imposed boundary conditions, and A_{znP} is a particular solution. (11-1) and (11-2) present the particular solutions in the PM magnetic field and armature reaction field, respectively.

$$A_{znpPM}=\begin{cases} A_{znpPM}=\dfrac{\mu_0 jnp_s rM_n}{1-(np)^2} & np_s\neq 1 \\ A_{znpPM}=\pm\mu_0\dfrac{jnp_s}{2}r\ \ln rM_n & np_s=\pm 1 \end{cases} \tag{11-1}$$

$$A_{znpAR}=\begin{cases} A_{znpPM}=\dfrac{\mu_0 jnp_s rM_n}{1-(np)^2} & np_s\neq 1 \\ A_{znpPM}=\pm\mu_0\dfrac{jnp_s}{2}r\ \ln rM_n & np_s=\pm 1 \end{cases} \tag{11-2}$$

Through these general solutions, the characteristic equation of the flux density in each region can be expressed. The boundary conditions used in the analytical

Table 1. Boundary Conditions

Region	PM	Armature	Radius	Boundary Conditions (Armature)		Boundary Conditions (PM)	
I	Rotor	Rotor	$r = R_0$	$A_{zn}^{I} = 0$		$A_{zn}^{I} = 0$	
			$r = R_{rc}$	$A_{rn}^{I} = A_{rn}^{II}$	$H_{\theta n}^{I} = H_{\theta n}^{II}$	$A_{rn}^{I} = A_{rn}^{II}$	$H_{\theta n}^{I} = H_{\theta n}^{II} - M_{\theta n}$
II	PM	Air	$r = R_{air}$	$A_{rn}^{II} = A_{rn}^{III}$	$H_{\theta n}^{II} = H_{\theta n}^{III}$	$A_{rn}^{II} = A_{rn}^{III}$	$H_{\theta n}^{II} - M_{\theta n} = H_{\theta n}^{III}$
III	Air	PM	$r = R_{co}$	$A_{rn}^{III} = A_{rn}^{IV}$	$H_{\theta n}^{III} = H_{\theta n}^{IV}$	$A_{rn}^{III} = A_{rn}^{IV}$	$H_{\theta n}^{III} = H_{\theta n}^{IV}$
IV	Stator	Stator	$r = R_{sc}$	$A_{rn}^{IV} = 0$		$A_{rn}^{IV} = 0$	

prediction of the magnetic vector potential due to the winding current are presented in Table 1. Applying those boundary conditions to the field equations results in the following matrix:

$$\mathbf{T}_{ex}\mathbf{X}_{ex} = \mathbf{U}_{ex} \tag{12}$$

Here T_{ex} is the coefficient matrix, and it can be solved by a computer program quickly and conveniently. Solving this matrix equation can determine the coefficients in terms of the magnetized distribution, as well as other material and dimensional parameters. With the derived general solution, the flux density distribution in the normal and tangential direction according to the contour lines in each region can be determined by (15).

$$B = \nabla \times A_{zn} = \frac{1}{r}\begin{pmatrix} \mathbf{i}_r & r\mathbf{i}_\theta & \mathrm{i}_z \\ \frac{\partial}{\partial r} & \frac{\partial}{\partial \theta} & \frac{\partial}{\partial z} \\ 0 & 0 & A_{zn}e^{jnp_s\theta} \end{pmatrix} = \frac{jnp}{r}A_{zn}e^{jnp_s\theta}\mathbf{i}_r - \frac{\partial}{\partial r}A_{zn}e^{jnp_s\theta}\mathbf{i}_\theta$$

$$B_{rn} = \frac{jnp_s}{r}A_{zn}e^{jnp_s\theta}\mathbf{i}_r,\ B_{\theta n} = -\frac{\partial}{\partial r}A_{zn}e^{jnp_s\theta}\mathbf{i}_\theta \tag{15}$$

2.4. Back-EMF

The back-EMF is given by the product of the angular velocity ω and the rate of change in the flux linkage with respect to the angular position; it is written as (16), where λ_f and η are the flux linkage and the coil pitch, respectively.

$$V_{emf} = -\frac{d}{dt}\lambda_f = N_t\frac{d}{dt}\left[\int_0^{\eta} G_r B_{zn}^{III} e^{jnp_s wt} d\theta\right] \tag{16}$$

2.5. Self- and Mutual Inductance

The self and mutual inductances are obtained from the energy relationship as

$$W = \frac{1}{2}L_{sm}i^2 = \frac{1}{2}\lambda i = \frac{1}{2}\int_v B \cdot H dv \tag{17}$$

The W can be divided into two components using the vector identity – the W_I component, associated with the boundary, and the W_{II} component, associated with the current carry – as follows:

$$W = W_I + W_{II} = \frac{1}{2}\int_s \nabla \times (A \times H) dv + \frac{1}{2}\int_v A \cdot J dv \tag{18}$$

Here, the surface integral is zero, since the surface encloses the volume containing all the magnetic energy, which requires that A and H be zero on the bounding surface. Hence, (19) can be defined as

$$W = \frac{1}{2}\int_v A \cdot J dv = \frac{l_a}{2}\int_0^{2\pi} A \cdot J r d\theta dr \tag{19}$$

Using (19), we can derive the self-inductance L_{sm} and mutual inductance L_M in one-phase winding. Thus, (20) can be derived [3].

$$L_{i,j} = 2\pi L_a \sum_{n=-\infty}^{\infty} A_{\mathrm{int}\_r} J e^{j\left(\frac{2\pi n(i-j)}{m}\right)} \tag{20}$$

Here, L_a is the active length of the machine, and $L_{i,j}$ is the self-inductance between phases when i is not equal to j. On the other hand, when i and j are equal, $L_{i,j}$ is the mutual inductance of a phase of winding.

3. Results and Discussion

3.1. Design specifications and manufactured model

Fig. 4 shows the manufactured model for experimental verification, which is a distributed winding type, four-pole, three-phase slotless permanent magnet motor, whose

Fig. 4. (Color online) Manufactured model of slotless PM motor.

Table 2. Design Specifications of Slotless PM Motor

Outer Stator Radius	26.5 [mm]	Inner Coil Radius	15.75 [mm]
Outer Rotor Radius	11.25 [mm]	Number of Poles	4
Outer PM Radius	13.75 [mm]	Output Power	1 [kW]
Stack Length	50 [mm]	Rated Speed	24000 [rpm]
Inner Stator Radius	20 [mm]	Rated Current	3.8 [A]
Inner Rotor Radius	4.5 [mm]	Rated Torque	4 [kg.cm]

design dimensions and specifications are listed in Table 2.

3.2. Magnetic Field, Back-EMF, and Inductance

Concentrated winding is usually used in a brushless dc (BLDC) motor driven by trapezoidal voltage, in which the coils are easily wound in the stator slots. The back-EMF voltage induced by this type of winding, however, contains many harmonic components. Distributed winding is usually used in a brushless AC (BLAC) machine driven by sinusoidal voltage, and its end-winding length is longer than that in the concentrated type of winding. This type of winding, however, achieves more sinusoidal back-EMF than the concentrated type of winding type [1, 2].

Fig. 5 shows a comparison of the back-EMF in concentrated winding and in distributed winding as obtained by the analytical method, FEM and measurements, and the results for its harmonic components, as shown in Fig. 6. The distributed winding type has a smaller THD value compared to the concentrated winding.

Fig. 7 and Fig. 8 show a comparison of the results of the normal and tangential components of the flux density as obtained by the FEM and the analytical method. The results are in good agreement for both components, which confirms the validity of the results presented in this paper.

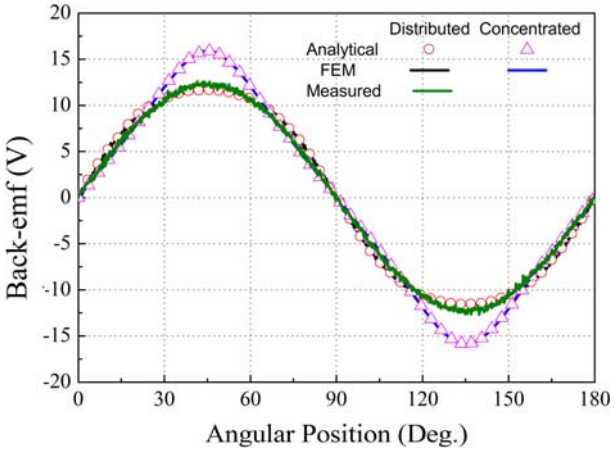

Fig. 5. (Color online) Comparison of back-EMF in distributed and concentrated types of winding.

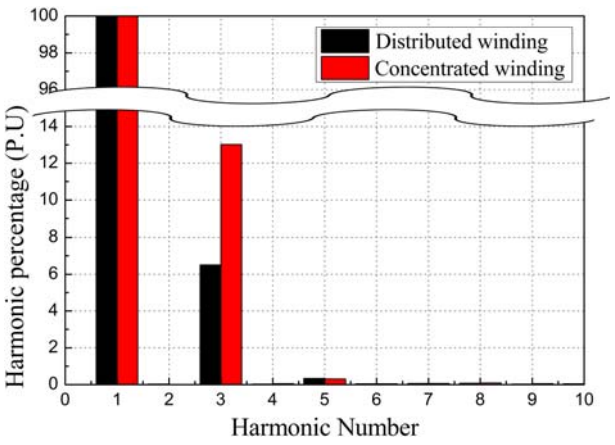

Fig. 6. (Color online) Comparison of harmonic components in distributed and concentrated types of winding.

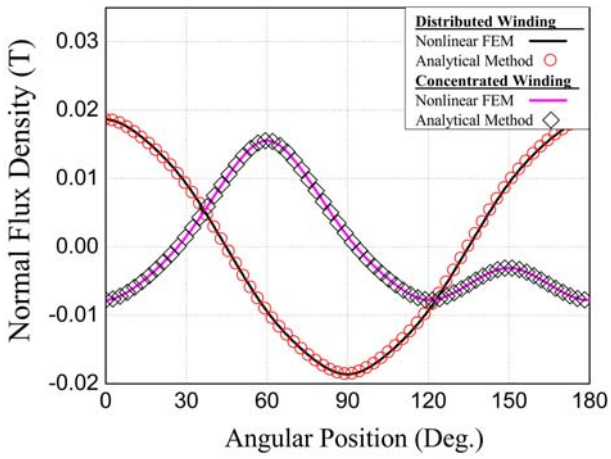

Fig. 7. (Color online) Normal flux density distribution at the air-gap center in distributed and concentrated types of winding.

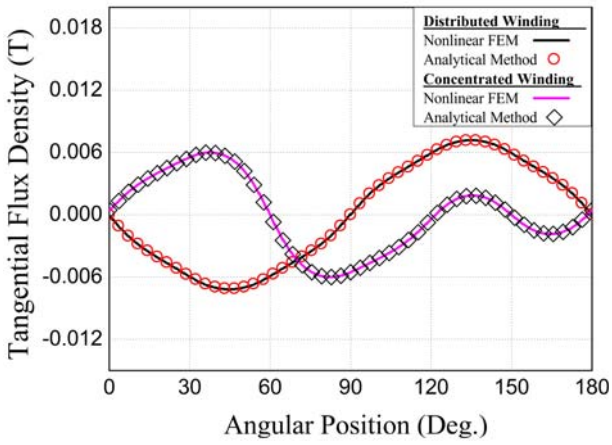

Fig. 8. (Color online) Tangential flux density distribution at the air-gap center in distributed and concentrated types of winding.

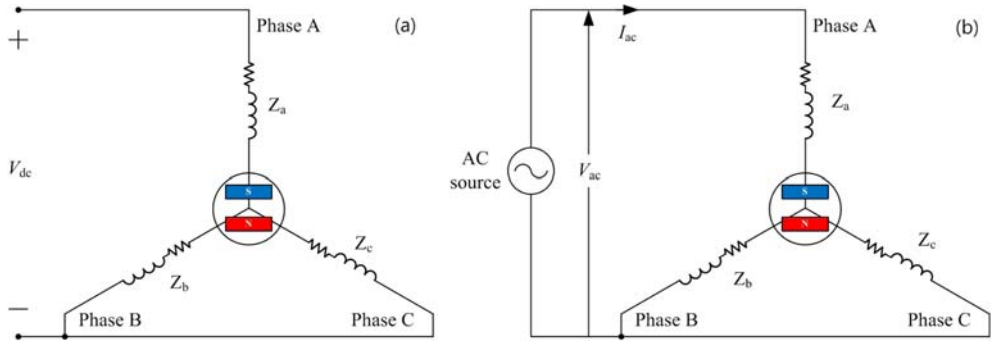

Fig. 9. (Color online) Concepts of AC standstill test for inductance measurement.

Table 3. Results of Winding Inductances

Winding	Analytical result		FEM result		Measured
	Self-Inductance	Mutual-Inductance	Self-Inductance	Mutual-Inductance	
Distributed	190.4[μH]	−75.80[μH]	191.6[μH]	−75.99[μH]	210.6[μH]
Concentrated	90.81[μH]	−25.16[μH]	91.95[μH]	−26.18[μH]	–

Fig. 9 shows concepts of AC standstill test for inductance measurement. First, for the d-axis alignment of the rotor, a positive DC voltage was applied to phase A, while the negative DC voltage was applied to phase B and C shown in Fig. 9(a). Then variable AC voltage is applied to the circuit shown in Fig. 9(b), voltage and current are measured. From these results, the winding inductances is obtained as (21) [12]

$$\frac{V_{ac}}{I_{ac}} = Z_a + Z_b \| Z_c = \frac{3}{2}\sqrt{R_a^2 + (w_e L)^2} \tag{21}$$

Table 3 compares the measured and predicted winding inductances. As can be seen in the table, the analytical results are in good agreement with the FEM results. However, the predicted winding inductances as compared to the measured inductance of the manufactured model show an error of approximately 9.6%. This is caused by the end turn inductance, which is not covered in this paper, and by a number of mechanical errors that emerged in the manufacturing process. As predicted in Table 3, it can be observed the inductance with concentrated winding is lower than that distributed winding about 47%.

4. Conclusion

This paper has presented an analytical approach to the magnetic field and inductances of a slotless permanent magnet (PM) machine with two types of winding. The distributed winding type has a smaller THD value and larger inductance value compared to the concentrated winding. The analytical procedure that was performed using the space harmonic method was validated by FEM and an experiment, whose results are in good agreement. Since this method can dramatically reduce the analysis time with high reliability, we believe that this paper can contribute to other related works, such as the initial design of permanent magnet machines according to design specifications.

References

[1] J. R. Melcher, Continuum Electro-Mechanics, The MIT Press, Cambridge (1981).
[2] R. Krishnan, Switched Reluctance Motor Drives, CRC Press, Boca Raton (2009).
[3] K. Atallah, Z. Q. Zhu, D. Howe, and T. S. Birch, IEEE Trans. Magn. **34**, 3737 (1998).
[4] Z. Q. Zhu and D. Howe, IEEE Trans. Magn. **29**, 136 (1993).
[5] Khai D. T. Ngo, E. Alpizar, and J. Kenneth Watson, IEEE Trans. Magn. **8**, 200 (1993).
[6] Z. Keyi, L. Bin, L. Zhiyuan, C. Shukang, and Z. Ruiping, IEEE Trans. Magn. **45**, 336 (2009).
[7] C. Ye, K. Yu, G. Zhang, and Y. Pan, IEEE Trans. Magn. **45**, 522 (2009).
[8] Z. Q. Zhu, D. Howe, E. Bolte, and B. Ackermann, IEEE Trans. Magn. **29**, 124 (1993).
[9] S.-M. Jang, H.-I. Park, J.-Y. Choi, K.-J. Ko, and S.-H. Lee, IEEE Trans. Magn. **47**, 3586 (2011).
[10] Y. S. Chen, Z. Q. Zhu, and D. Howe, IEEE Trans. Energy Convers. **14**, 686 (1999).
[11] O. Wallmark, and P. Kjellqvist, IEEE Trans. Energy Convers. **24**, 841 (2009).
[12] J.-Y. Choi, Y.-S. Park, and S.-M. Jang, IEEE Trans. Magn. **48**, 987 (2012).